Applied Physics Letters

RESEARCH ARTICLE | MARCH 03 2023

Low-frequency noise in ZrS_3 van der Waals semiconductor nanoribbons

Special Collection: Electronic Noise: From Advanced Materials to Quantum Technologies

A. Rehman ; G. Cywinski ; W. Knap; J. Smulko ; A. A. Balandin ; S. Rumyantsev

Appl. Phys. Lett. 122, 090602 (2023)
https://doi.org/10.1063/5.0143641
CHORUS

AIP Publishing

Applied Physics Letters ARTICLE scitation.org/journal/apl

Low-frequency noise in ZrS_3 van der Waals semiconductor nanoribbons

Cite as: Appl. Phys. Lett. **122**, 090602 (2023); doi: 10.1063/5.0143641
Submitted: 25 January 2023 · Accepted: 18 February 2023 ·
Published Online: 3 March 2023

A. Rehman,[1,a)] G. Cywinski,[1] W. Knap,[1] J. Smulko,[2] A. A. Balandin,[3] and S. Rumyantsev[1,a)]

AFFILIATIONS

[1]CENTERA Laboratories, Institute of High-Pressure Physics, 01-142 Warsaw, Poland
[2]Department of Metrology and Optoelectronics, Faculty of Electronics, Telecommunications, and Informatics, Gdańsk University of Technology, Gdańsk, Poland
[3]Department of Electrical and Computer Engineering, University of California, Riverside, California 92521, USA

Note: This paper is part of the APL Special Collection on Electronic Noise: From Advanced Materials to Quantum Technologies.
[a)]**Authors to whom correspondence should be addressed:** adilrehhman@gmail.com and roumis4@gmail.com

ABSTRACT

We report the results of the investigation of low-frequency electronic noise in ZrS_3 van der Waals semiconductor nanoribbons. The test structures were of the back-gated field-effect-transistor type with a normally off *n*-channel and an on-to-off ratio of up to four orders of magnitude. The current–voltage transfer characteristics revealed significant hysteresis owing to the presence of deep levels. The noise in ZrS_3 nanoribbons had spectral density $S_I \sim 1/f^{\gamma}$ (f is the frequency) with $\gamma = 1.3$–1.4 within the whole range of the drain and gate bias voltages. We used light illumination to establish that the noise is due to generation–recombination, owing to the presence of deep levels, and determined the energies of the defects that act as the carrier trapping centers in ZrS_3 nanoribbons.

After the invention of graphene, it was soon realized that many other layered materials can be exfoliated or grown in the form of low-dimensional structures. Among them are transition metal dichalcogenides and trichalcogenides, which can form two-dimensional (2D) and one-dimensional (1D) structures of one or a few atomic layers or chains, respectively.[1] In transition metal dichalcogenides, weak van der Waals (vdW) force binds individual 2D atomic layers, and in transition metal trichalcogenides, the vdW force binds 1D atomic chains.[2–5] Therefore, these materials are known as 2D and 1D vdW materials. The low-dimensional structures reveal a wide spectrum of properties, from metallic to wide-bandgap semiconducting. Many 2D dichalcogenides, e.g., MoS_2, $MoSe_2$, and WS_2, have already been studied in detail (see Refs. 6–8 and references therein). The 1D trichalcogenides are much less explored systems. The existing reports mainly focus on synthesis methods, electron and phonon band structure calculations, and optical properties.[9–11] With the exception of TiS_3,[12] the electrical properties of 1D vdW semiconductors have not been systematically studied. The investigated metallic 1D vdW nanoribbons of $TaSe_3$ and $ZrTe_3$ revealed exceptionally high current densities of the order of 10–100 MA cm^{-2}.[13–15] The mechanism of light-enhanced gas sensing by ZrS_3 nanoribbons was studied in Ref. 16. The polymer composites with low loadings of quasi-1D $TaSe_3$ nanoribbon fillers (<3 vol. %) demonstrated excellent electromagnetic interference shielding within the frequency range from the X-band to subterahertz frequencies while remaining DC electrically insulating.[17] The promising results obtained for 1D vdW metallic nanoribbons motivate the investigation of the 1D vdW semiconductors for potential electronic applications.

For electronic devices, the level of electrical noise, particularly low-frequency noise, is important. We are aware of only a few reports on the noise properties of vdW quasi-1D trichalcogenides nanowires. The noise properties of $TaSe_3$ metallic nanowires were studied in Ref. 18. It was found that $TaSe_3$ nanowires have lower levels of noise compared to carbon nanotubes and graphene. The temperature-dependent measurements revealed that the $1/f$ (f is the frequency) noise mechanism in $TaSe_3$ complies with the Dutta–Horn model.[19] Low-frequency noise investigation of $ZrTe_3$ nanoribbons found the $1/f$ noise behavior near room temperature (RT) and generation–recombination (G–R) noise at low temperatures.[20] The corner frequency of the G–R noise was found to be dependent on the applied voltage. This effect was explained by the Frenkel–Poole mechanism. The low-frequency noise in 1D $(TaSe_4)_2I$ Weyl semimetal nanoribbons and its relation to the Peierls phase transition was reported in Ref. 21. The available studies of ZrS_3 vdW semiconductors

are mainly focused on the optical properties of bulk crystals[22–26] and exfoliated nanoribbons.[27–30] Here, we report on the experimental study of low-frequency noise in ZrS_3 nanoribbons and its theoretical analysis, which allowed us to determine a number of interesting characteristics of this material, important for future electronic applications.

The crystal structure of ZrS_3, as of many other trichalcogenides, insures the anisotropy of its mechanical and electrical properties in all three directions. Such vdW materials exfoliate not in the form of rectangular or circular nanowires but rather into ribbons with widths larger than their thicknesses. The crystals of ZrS_3 can be grown by a chemical vapor transport technique.[17,31] More details about the synthesis method and material characterization data can be found in Ref. 32. The quasi-1D ZrS_3 nanoribbons for the test structures were prepared by mechanical exfoliation on Si/SiO_2 substrates using a transfer system with micro-manipulators. The field-effect-transistor (FET) type structures were fabricated by standard e-beam lithography and e-beam metal evaporation. Figure 1(a) shows a schematic view of the studied ZrS_3 nanoribbon device along with a DC biasing scheme. The optical image of the fabricated test structure based on the exfoliated and transferred ZrS_3 nanoribbon is shown in the inset in Fig. 1(b). Five contacts formed four samples of width (W_G) $\approx 2.2\ \mu$m and length (L_G) $\approx 1.3\ \mu$m. The low-frequency electronic noise was measured in a frequency range from 0.5 to 100 Hz. The noise spectral density of voltage fluctuations (S_V) was measured across a load resistor (R_L) amplified by a low-noise amplifier and analyzed by a dynamic signal analyzer. The voltage-referred noise spectral density (S_V) was converted into a noise spectral density of the short circuit current fluctuations (S_I) by using the equation $S_I = S_V(\frac{R_D+R_L}{R_D\times R_L})^2$, where R_D is the device resistance.

Figure 1(b) presents an example of the transfer current–voltage characteristics of the ZrS_3 nanoribbon FET measured in the dark at RT. The arrows in Fig. 1(b) show the directions of the forward and reverse voltage sweeps. The drain current (I_D) increases with increasing gate voltage (V_G) demonstrating a normally off n-channel FET behavior with a threshold voltage (V_{th}) around ~14 V for the forward voltage sweep. All four studied devices demonstrated a similar

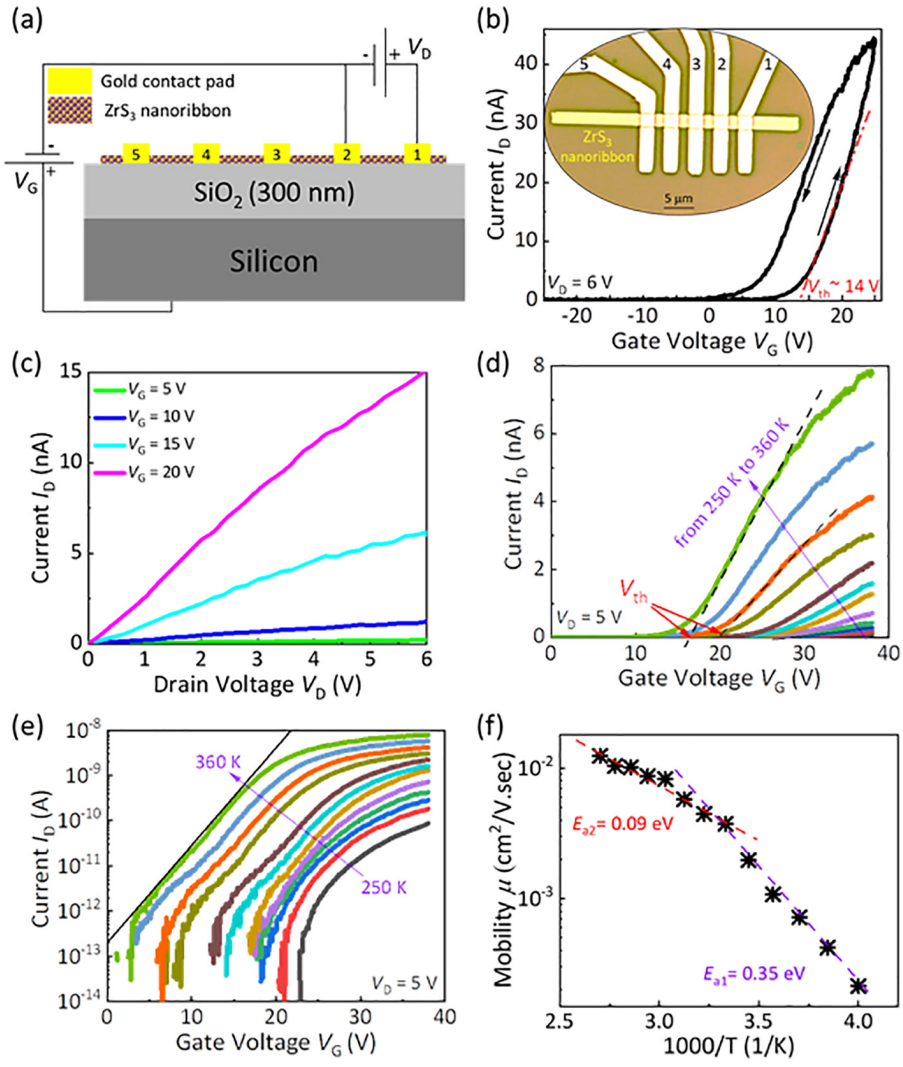

FIG. 1. (a) Schematic of a studied device for one pair of the contacts along with DC biasing scheme. (b) Transfer current–voltage characteristics of a representative device at room temperature (1–2 pairs of contacts). Arrows indicate the direction of the voltage sweep. The inset shows an optical microscopy image of a studied device. Each pair of contacts forms a separate FET with $W_G \times L_G \approx 2.2 \times 1.3\ \mu$m of total area. (c) Output current–voltage characteristics at different gate voltages. Transfer current–voltage characteristics of a device over a wide range of temperatures in (d) linear and (e) semi-logarithmic scales. (f) Arrhenius plot of the mobility temperature dependence.

behavior with the threshold voltage varied between 12 and 25 V. The presence of a significant hysteresis of the transfer characteristic was attributed to the charge traps at the SiO_2/ZrS_3 interface and inside the nanoribbon. Similar transfer characteristics were reported in Refs. 30 and 31. Typical output current–voltage characteristics at different gate voltages are presented in Fig. 1(c). These characteristics are linear at low drain voltage (V_D) with the tendency to sub-linearity at higher voltage, as expected for a conventional FET. The linearity at small drain voltages indicates reasonably good Ohmic contacts. The transfer characteristics in a forward voltage sweep of a representative device at different temperatures are shown in Fig. 1(d). One can notice the linear regions at the medium gate voltages and the trend to saturate at high gate voltages, where the contact resistance starts to contribute to the overall drain-to-source resistance.

The measured transfer characteristics depend strongly on temperature [see Fig. 1(d)]. The threshold voltage decreases and the slope of the linear part of the characteristic increases with increasing temperature. To make the trends clearer, the current–voltage transfer characteristics at different temperatures are shown in the semi-logarithmic scale in Fig. 1(e). One can see the on-to-off ratio of about four orders of magnitude. The average subthreshold slope of the exponential dependence, $I_D \propto \exp(qV_G/\eta kT)$, is characterized by a relatively high factor $\eta \cong 60$ at $T = 360$ K (here, q is the elementary charge, and k is the Boltzmann's factor). One can also notice dips on the exponential part of the characteristics, which can be explained by the presence of a deep level. The linear regions of the characteristics shown in Fig. 1(d) are defined by the electron concentration and the mobility. The field-effect mobility can be found as

$$\mu_{FE} = \frac{dI_D}{dV_G}\frac{1}{CV_D}\frac{L_G}{W_G}. \quad (1)$$

Here, $C = \varepsilon_0\varepsilon/d$ is the capacitance per unit area, ε_0 is the permittivity of a vacuum, and ε and d are the relative permittivity and thickness of the silicon dioxide, respectively. Figure 1(f) shows the Arrhenius plot for the mobility temperature dependence, which yields two activation energies of $E_{a1} = 0.09$ and $E_{a2} = 0.35$ eV.

The low-frequency noise spectra of current fluctuations in ZrS_3 nanoribbon structures at different drain voltages and under dark conditions are shown in Fig. 2(a). At all biases, both in the weak and strong inversion, the spectra have the $1/f^{\gamma}$ noise shape with the exponent $\gamma \cong 1.3$–1.4, weakly dependent on the drain and gate voltages. The drain–voltage dependence of the noise spectral density (S_I) at $V_G = 5$ V is presented in the inset in Fig. 2(a). One can see that S_I is proportional to V_{D^2}, which implies that resistance fluctuations (δR) are responsible for the $1/f$ noise and the drain current makes these fluctuations visible. The low-frequency noise in the majority of semiconductor FETs complies with the number of carriers' fluctuations mechanism, described by the McWhorter model.[33,34] However, this is not always the case for low-dimensional vdW materials. For example, it was recently demonstrated that the $1/f$ noise in h-BN encapsulated graphene can be dominated by the mobility fluctuations.[35] In accordance with the McWhorter model, the $1/f$ noise originates from the tunneling of carriers from the channel to the traps in the gate dielectric. The relative spectral noise density of the drain current fluctuations at the linear part of the transfer current–voltage characteristic is given by the following equation:[34]

$$\frac{S_I}{I_D^2} = \frac{kTN_t}{\alpha f W_G L_G n_s^2}, \quad (2)$$

where N_t is the effective trap density, n_s is the carrier concentration, and α is the attenuation coefficient of the electron wave function under the barrier ($\sim 10^8\,\mathrm{cm}^{-1}$). The input gate voltage noise (S_{Vg}) in the McWhorter model can be found as

$$S_{Vg} = \frac{S_I}{I_D^2}\frac{I_D^2}{g_m^2} = \frac{kTN_t q^2}{\alpha f W_G L_G C^2}, \quad (3)$$

where g_m is the transconductance. Both, Eqs. (2) and (3), can be used to estimate the effective trap density (N_t) responsible for the $1/f$ noise. Equation (3) is preferable because it does not contain the concentration (n_s) and the uncertainty in this parameter is eliminated. Another advantage of Eq. (3) is that unlike the noise spectral density (S_I), the input gate voltage noise (S_{Vg}) is not affected by the contact resistance.[36]

The dependence of the noise spectral density (S_{Vg}) on the gate voltage in the ZrS_3 nanoribbon FETs is shown in Fig. 2(b). As one can notice, S_{Vg} does not depend on the gate voltage, which is in line with the McWhorter model [see Eq. (3)]. The extracted effective trap density from Eq. (3) yields $N_t \sim 3 \times 10^{22}\,\mathrm{eV}^{-1}\,\mathrm{cm}^{-3}$. This value looks unrealistically high. The ZrS_3 nanoribbon test structures were prepared using high-quality SiO_2/Si wafers and there are no reasons for such a high trap density in the SiO_2 layer. This suggests that the actual noise mechanism differs from the conventional McWhorter model. Most likely, the traps associated with the defects, which are responsible

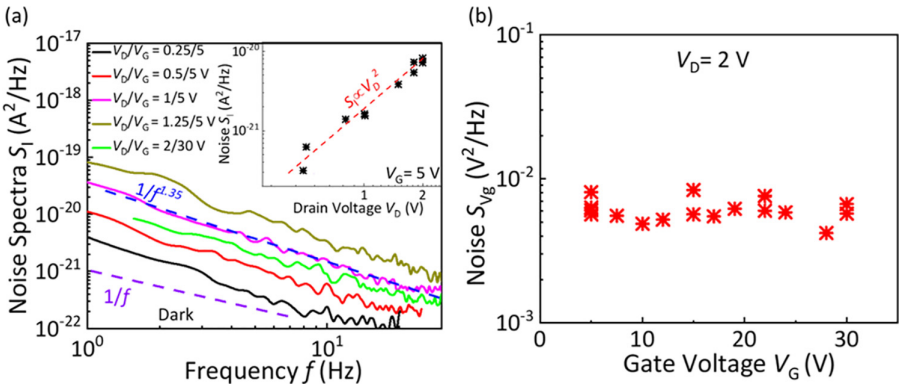

FIG. 2. (a) Low-frequency noise spectra (S_I) of a studied device at different bias voltages under dark conditions. The inset shows the dependence of the spectral density of the current fluctuations on the drain voltage at $f = 10$ Hz. (b) Input gate voltage noise spectral density as a function of the gate voltage at $f = 10$ Hz.

for noise, are located not in the oxide layer but inside the nanoribbon. Probably the same traps are responsible for hysteresis on the current–voltage characteristics. In this case, the extracted trap density should be considered as a noise figure of merit and called an *effective* trap density. This observation can be extended to other vdW materials and devices fabricated by the transfer of ribbons. In this case, the extracted trap density should be considered as a noise figure of merit and called an *effective* trap density, which can be used as the metric for the material and interface quality. This observation can be extended to other vdW materials and devices fabricated by the transfer method. The specific rate of the noise scaling with R_D in our quasi-1D material is different from the dependence $S_I/I_D^2 @ 10^{-11}R_D$ proposed in Ref. 37 on the basis of experimental data for carbon nanotubes. Our experimental results comply well with the dependence $S_I/I_D^2 = 2\times10^{-21}\ R_D^2$. Therefore, one can see that noise in ZrS_3 semiconductor nanoribbons is smaller than that in carbon nanotubes at $R_D < 5\,G\Omega$.

One of the advanced methods to study the nature of the $1/f$ noise in semiconductors is the noise measurements under light illumination. The theory of the influence of light on the $1/f$ noise in semiconductors was developed in Ref. 38 (see also review in Ref. 39 and references therein). In accordance with this model, the $1/f$ noise originates from the fluctuations in the number of carriers due to the fluctuations of the occupancy of trap levels responsible for noise. The illumination can change the occupancy of these levels, and as a result, modify the noise spectrum. In order to form the $1/f$ spectrum, one requires several trap levels with different characteristic times or a continuous spectrum of the density of state tails near the band edges as it was assumed in Ref. 38. The spectral noise density of the G–R noise due to a single level is given by

$$\frac{S_I}{I_D^2} = \frac{4N_{tl}\,\tau_c F^2(1-F)}{Vn^2\,1+(\omega\tau_c F)^2}, \tag{4}$$

where N_{tl} is the trap concentration, V is the sample volume, F is the occupancy of the level, $\tau_c = (\sigma n v)^{-1}$ is the capture time, σ is the capture cross section, v is the thermal velocity, n is the volume electron concentration, and $\omega = 2\pi f$ is the circular frequency (see Ref. 40 and references therein). It is clear from Eq. (4) that the normalized noise spectral density (S_I/I_D^2) depends non-monotonically on the occupancy function (F) and, therefore, on the intensity of light. One can also see from Eq. (4) that different levels with different occupancy functions in the dark should respond differently to illumination. As a result, the shape of the noise spectra should depend on the illumination. This effect was also observed for conventional semiconductors such as GaAs, Si (see review in Ref. 40 and reference therein), and GaN nanowires.[41] It was found that illumination reduces the slope of the $1/f^\gamma$ spectrum making it flatter (i.e., reducing the exponent γ). We studied noise in the ZrS_3 nanoribbons under illumination from the microscope incandescent bulb powered from a DC power source. This kind of bulb has a significant part of the emission spectra in the visible range of the spectra that correspond to the ZrS_3 bandgap of $E_g \sim 1.8$–2.0 eV (~2.0 eV corresponds to red light).[42–44] Therefore, this band-to-band illumination creates electrons and holes. Minority carriers, holes in this case, can be captured by the trap levels responsible for the noise. As a result, the occupancy of the traps changes.[39] We found that both resistance and low-frequency noise are strongly sensitive to illumination. Figure 3(a) shows the normalized noise spectral density (S_I/I_D^2) in the dark environment and under illumination measured at high gate voltage of $V_G = 30$ V (strong inversion). As expected, the shape of the noise spectra changes. It is important that illumination decreases the noise at low frequencies. Therefore, the change in the noise spectra cannot be explained by the noise of the light source. Contrary to the previous studies of noise under illumination in conventional semiconductors, Si and GaAs,[39] the effect of light on ZrS_3 nanoribbons was observed under the condition of high photoconductivity. Therefore, an increase in the electron concentration contributes to the effect of light on noise [see Eq. (4)]. To exclude this effect, we analyzed the noise spectral density (S_I), which does not depend on electron concentration and is given by

$$S_I = \frac{4N_{tl}q^2\mu^2V_D^2A\tau_cF^2(1-F)}{L_G^3\left(1+\omega^2\tau_c^2F^2\right)}, \tag{5}$$

where $A = W_G h$ is the sample cross section and h is the thickness of the ribbon. Figure 3(b) shows the dependences of the noise spectral density (S_I) on the light intensity adjusted by the power supplied to the bulb. The higher the frequency the stronger the effect of light is on noise. At the lowest frequency of $f = 0.5$ Hz, illumination does not affect the noise. If we assume that the shape of the spectra is the same at even lower frequencies, noise reduction at $f < 0.5$ Hz will be expected. The strong effect of illumination on noise is a solid argument that noise in ZrS_3 nanoribbons is due to the trap levels.

In conclusion, we investigated low-frequency electronic noise in ZrS_3 vdW nanoribbons. The test structures were of the back-gated field-effect-transistor type with a normally off n-channel and an on-to-off ratio of up to four orders of magnitude. The noise in ZrS_3 nanoribbons has spectral density $S_I \sim 1/f^\gamma$ (f is the frequency) with

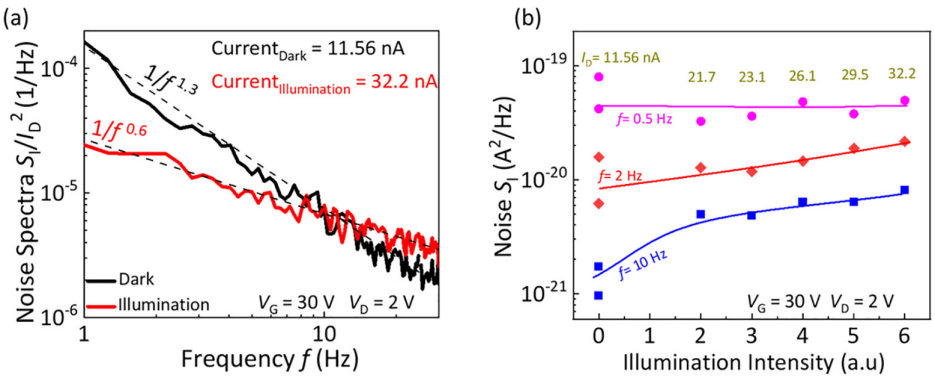

FIG. 3. (a) Noise spectra (S_I/I_D^2) of the studied device in a dark environment and under illumination. (b) Dependences of the noise spectral density (S_I) on the illumination intensity, in arbitrary units at different frequencies. The current shown next to the experimental points is the drain current, which can serve as a measure of the light intensity.

$\gamma = 1.3–1.4$ within the whole range of the drain and gate bias voltages. We used temperature-dependent measurements and light illumination to establish that the noise is of generation–recombination origin, owing to the presence of deep levels in ZrS_3 nanoribbons. We established the energies of the defects, which act as the carrier trapping centers. The results contribute to understanding the carrier transport in the new type of quasi-1D semiconductors and are important for their future applications. They also extend the use of the low-frequency noise spectroscopy for material quality assessment to a range of 1D vdW materials.

The work was supported by the CENTERA Laboratories in the framework of the International Research Agendas program for the Foundation for Polish Sciences, co-financed by the European Union under the European Regional Development Fund (No. MAB/2018/9). A.A.B. acknowledges partial support from the National Science Foundation (NSF) program Designing Materials to Revolutionize and Engineer our Future (DMREF) via Project No. DMR-1921958. J.S. acknowledges partial support from the National Science Centre, Poland, Project No. 2019/35/B/ST7/02370, "System of gas detection by two-dimensional materials."

AUTHOR DECLARATIONS

Conflict of Interest

The authors have no conflicts to disclose.

Author Contributions

Adil Rehman: Formal analysis (equal); Investigation (lead). **Grzegorz Cywiński:** Resources (equal); Writing – review & editing (equal). **Wojciech Maciej Knap:** Funding acquisition (lead); Writing – review & editing (equal). **Janusz Smulko:** Formal analysis (equal); Writing – review & editing (equal). **Alexander A. Balandin:** Formal analysis (equal); Writing – review & editing (equal). **Sergey L. Rumyantsev:** Supervision (lead); Writing – original draft (equal).

DATA AVAILABILITY

The data that support the findings of this study are available from the corresponding authors upon reasonable request.

REFERENCES

[1]A. A. Balandin, F. Kargar, T. T. Salguero, and R. K. Lake, Mater. Today **55**, 74 (2022).
[2]M. A. Bloodgood, Y. Ghafouri, P. Wei, and T. T. Salguero, Appl. Phys. Lett. **120**(17), 173103 (2022).
[3]I. Gorlova, S. Nikonov, S. Zybtsev, V. Y. Pokrovskii, and A. Titov, Appl. Phys. Lett. **120**(15), 153102 (2022).
[4]F. Kargar, Z. Barani, N. R. Sesing *et al.*, Appl. Phys. Lett. **121**(22), 221901 (2022).
[5]A. Sinchenko, R. Ballou, J. Lorenzo, T. Grenet, and P. Monceau, Appl. Phys. Lett. **120**(6), 063102 (2022).
[6]V. Shanmugam, R. A. Mensah, K. Babu, S. Gawusu, A. Chanda, Y. Tu, R. E. Neisiany, M. Försth, G. Sas, and O. Das, Part. Part. Syst. Charact. **39**, 2200031 (2022).
[7]Y. Liu, N. O. Weiss, X. Duan, H.-C. Cheng, Y. Huang, and X. Duan, Nat. Rev. Mater. **1**(9), 10642 (2016).
[8]D. L. Duong, S. J. Yun, and Y. H. Lee, ACS Nano **11**(12), 11803 (2017).
[9]J. O. Island, A. J. Molina-Mendoza, M. Barawi, R. Biele, E. Flores, J. M. Clamagirand, J. R. Ares, C. Sánchez, H. S. Van Der Zant, and R. D'Agosta, 2D Mater. **4**(2), 022003 (2017).
[10]Y. Sugita, T. Miyake, and Y. Motome, Physica B **536**, 48 (2018).
[11]A. Patra and C. S. Rout, RSC Adv. **10**, 36413 (2020).
[12]N. Tripathi, V. Pavelyev, P. Sharma, S. Kumar, A. Rymzhina, and P. Mishra, Mater. Sci. Semicond. Process. **127**, 105699 (2021).
[13]M. A. Stolyarov, G. Liu, M. A. Bloodgood, E. Aytan, C. Jiang, R. Samnakay, T. T. Salguero, D. L. Nika, S. L. Rumyantsev, and M. S. Shur, Nanoscale **8**(34), 15774 (2016).
[14]A. Geremew, M. Bloodgood, E. Aytan, B. Woo, S. Corber, G. Liu, K. Bozhilov, T. Salguero, S. Rumyantsev, and M. Rao, IEEE Electron Device Lett. **39**(5), 735 (2018).
[15]T. A. Empante, A. Martinez, M. Wurch, Y. Zhu, A. K. Geremew, K. Yamaguchi, M. Isarraraz, S. Rumyantsev, E. J. Reed, and A. A. Balandin, Nano Lett. **19**(7), 4355 (2019).
[16]K. Drozdowska, A. Rehman, S. Rumyantsev, M. Wurch, L. Bartels, A. Balandin, J. Smulko, and G. Cywiński, Mater. Today Commun. **34**, 105379 (2023).
[17]Z. Barani, F. Kargar, Y. Ghafouri, S. Ghosh, K. Godziszewski, S. Baraghani, Y. Yashchyshyn, G. Cywiński, S. Rumyantsev, and T. T. Salguero, Adv. Mater. **33**(11), 2007286 (2021).
[18]G. Liu, S. Rumyantsev, M. A. Bloodgood, T. T. Salguero, M. Shur, and A. A. Balandin, Nano Lett. **17**(1), 377 (2017).
[19]P. Dutta and P. Horn, Rev. Mod. Phys. **53**(3), 497 (1981).
[20]A. K. Geremew, S. Rumyantsev, M. A. Bloodgood, T. T. Salguero, and A. A. Balandin, Nanoscale **10**(42), 19749 (2018).
[21]S. Ghosh, F. Kargar, N. R. Sesing, Z. Barani, T. T. Salguero, D. Yan, S. Rumyantsev, and A. A. Balandin, Adv. Electron. Mater. **9**, 2200860 (2022).
[22]S. Kurita, J. Staehli, M. Guzzi, and F. Lévy, Physica B + C **105**(1–3), 169 (1981).
[23]S. Srivastava and B. Avasthi, J. Mater. Sci. **27**(14), 3693 (1992).
[24]A. Ait-Ouali and S. Jandl, Phys. Rev. B **49**(3), 1813 (1994).
[25]A. Patel, C. Limberkar, K. Patel, S. Bhakhar, K. Patel, G. Solanki, and V. Pathak, Sens. Actuators A **331**, 112969 (2021).
[26]L. Brattas and A. Kjekshus, Acta Chem. Scand. **26**(9), 3441 (1972).
[27]Y. R. Tao, X. C. Wu, and W. W. Xiong, Small **10**(23), 4905 (2014).
[28]A. Pant, E. Torun, B. Chen, S. Bhat, X. Fan, K. Wu, D. P. Wright, F. M. Peeters, E. Soignard, and H. Sahin, Nanoscale **8**(36), 16259 (2016).
[29]S. J. Gilbert, H. Yi, J.-S. Chen, A. J. Yost, A. Dhingra, J. Abourahma, A. Lipatov, J. Avila, T. Komesu, and A. Sinitskii, ACS Appl. Mater. Interfaces **12**(36), 40525 (2020).
[30]J. Guo, J. Tao, Z. Zhang, L. Fei, D. Li, J. Jadwiszczak, X. Wang, Y. Guo, X. Liao, and Y. Zhou, ACS Appl. Electron. Mater. **2**(11), 3756 (2020).
[31]D. S. Muratov, V. O. Vanyushin, N. S. Vorobeva, P. Jukova, A. Lipatov, E. A. Kolesnikov, D. Karpenkov, D. V. Kuznetsov, and A. Sinitskii, J. Alloys Compd. **815**, 152316 (2020).
[32]W. Kong, C. Bacaksiz, B. Chen, K. Wu, M. Blei, X. Fan, Y. Shen, H. Sahin, D. Wright, D. S. Narang, and S. Tongay, Nanoscale **9**(12), 4175 (2017).
[33]A. McWhorter and R. Kingston, *Semiconductor Surface Physics* (University of Pennsylvania, Philadelphia, 1957), p. 207.
[34]S. Christensson, I. Lundström, and C. Svensson, Solid-State Electron. **11**(9), 797 (1968).
[35]A. Rehman, J. A. D. Notario, J. S. Sanchez, Y. M. Meziani, G. Cywiński, W. Knap, A. A. Balandin, M. Levinshtein, and S. Rumyantsev, Nanoscale **14**(19), 7242 (2022).
[36]P. Sai, J. Jorudas, M. Dub, M. Sakowicz, V. Jakštas, D. But, P. Prystawko, G. Cywinski, I. Kašalynas, and W. Knap, Appl. Phys. Lett. **115**(18), 183501 (2019).
[37]P. G. Collins, M. Fuhrer, and A. Zettl, Appl. Phys. Lett. **76**(7), 894 (2000).
[38]N. D'yakonova and M. Levinshtein, Sov. Phys. Semicond. **23**(7), 743 (1989).
[39]N. D'yakonova, M. Levinshtein, and S. Rumyantsev, Sov. Phys. Semicond. **25**(2), 217 (1991).
[40]M. Levinshtein and S. Rumyantsev, Semicond. Sci. Technol. **9**(6), 1183 (1994).
[41]S. Rumyantsev, M. Shur, M. Levinshtein, A. Motayed, and A. Davydov, J. Appl. Phys. **103**(6), 064501 (2008).
[42]Y. Jin, X. Li, and J. Yang, Phys. Chem. Chem. Phys. **17**(28), 18665 (2015).
[43]C. Wang, C. Zheng, and G. Gao, J. Phys. Chem. C **124**(12), 6536 (2020).
[44]B. Mortazavi, F. Shojaei, M. Yagmurcukardes, M. Makaremi, and X. Zhuang, Energies **15**(15), 5479 (2022).